Mon. Not. R. Astron. Soc. **377,** 1638–1646 (2007) doi:10.1111/j.1365-2966.2007.11724.x

Early afterglow detection in the *Swift* observations of GRB 050801

Massimiliano De Pasquale,[1⋆] S. R. Oates,[1] M. J. Page,[1] D. N. Burrows,[2] A. J. Blustin,[1] S. Zane,[1] K. O. Mason,[1] P. W. A. Roming,[2] D. Palmer,[3] N. Gehrels[4] and B. Zhang[5]

[1]*Mullard Space Science Laboratory, University College London, Holmbury St Mary, Dorking Surrey RH5 6NT*
[2]*Department of Astronomy and Astrophysics, Pennsylvania State University, 525 Davey Laboratory, University Park, PA 16802, USA*
[3]*Los Alamos National Laboratories, Los Alamos, NM 87545, USA*
[4]*Goddard Space Flight Center, NASA, Greenbelt, MD 20771, USA*
[5] *Department of Physics, University of Nevada, Las Vegas, NV 89154, USA*

Accepted 2007 March 12. Received 2007 February 19; in original form 2006 July 21

ABSTRACT

We present results of *Swift* optical, ultraviolet (UV) and X-ray observations of the afterglow of GRB 050801. The source is visible over the full optical, UV and X-ray energy range of the *Swift* Ultraviolet and Optical Telescope and X-ray telescope instruments. Both optical and X-ray light curves exhibit a broad plateau ($\Delta t/t \sim 1$) during the first few hundred seconds after the γ-ray event. We investigate the multiwavelength spectral and timing properties of the afterglow, and we suggest that the behaviour at early times is compatible with an energy injection by a newly born magnetar with a period of a few tenths of a millisecond, which keeps the forward shock refreshed over this short interval by irradiation. Reverse shock emission is not observed. Its suppression might be due to GRB ejecta being permeated by high magnetic fields, as expected for outflows powered by a magnetar. Finally, the multiwavelength study allows a determination of the burst redshift, $z = 1.56$.

Key words: gamma-rays: bursts.

1 INTRODUCTION

The *Swift* mission represents a major breakthrough for the study of gamma-ray bursts (GRBs). New bursts are detected by the Burst Alert Telescope (BAT, Barthelmy et al. 2005), a coded-mask imager with higher sensitivity than that of the BATSE instrument onboard the Compton Gamma-Ray Observatory. *Swift* can begin observing a GRB with the X-ray telescope (XRT, Burrows et al. 2005) and Ultraviolet and Optical Telescope (UVOT, Roming et al. 2005) within ∼1 minute of the GRB onset, because of *Swift*'s unprecedented capability of fast and autonomous repointing. *Swift* has therefore enabled us to routinely explore these sources from the end of the prompt emission and the beginning of the afterglow, an epoch which was poorly known before this mission. The observations with the XRT and UVOT telescopes are addressing a series of key issues in GRB studies, such as the link between the γ-ray and the afterglow emission, the mechanisms which produce them, the duration and the properties of the 'central engine', and the origin of the prompt optical emission.

In this paper, we focus on GRB 050801. Among the bursts observed by *Swift*, this GRB was the first to have an early afterglow characterized by a peculiar phase of steady flux, both in the X-ray and in the Optical/UV, lasting a few hundred seconds. We will show that this distinguishing behaviour might be explained if we assume that the burst ejecta receive an injection of energy from a magnetar, born in the event that caused the GRB, with an initial period of a fraction of milliseconds.

GRB 050801 could thus be another example, in addition to GRB 051221 (Fan & Xu 2006), of a GRB with a magnetar as central engine.

2 PROMPT EMISSION

This burst was detected by the *Swift* satellite on 2005 August 1 at 18:28:16 UT. The γ-ray light curve registered by BAT (15–350 keV) shows two peaks, with a duration $t_{90} = 20 \pm 2$s (see Fig. 1). Henceforth errors are at the 68 per cent confidence level (C.L.), unless otherwise stated. The spectral analysis was performed only in the 15–150 keV band, because this is the band in which BAT has the optimal sensitivity. We tried the band, cut-off power law and simple power-law models to fit the data. None of them gave a fit significantly better than the others. However, the parameters in the first two are poorly constrained. We have therefore adopted the results of the simple power-law model fit, which gives a spectral index $\beta = -1.00 \pm 0.16$ with a reduced chi-squared of $\chi_\nu = 1.43$ with 73 degrees of freedom. The total fluence in the 15–150 keV band is 2.88×10^{-7} erg cm^{-2}, which allows us to classify this burst as moderately faint. Interestingly, the second peak is softer than the first one, being visible only at energies lower than ∼50 keV. In the following,

⋆E-mail: mdp@mssl.ucl.ac.uk

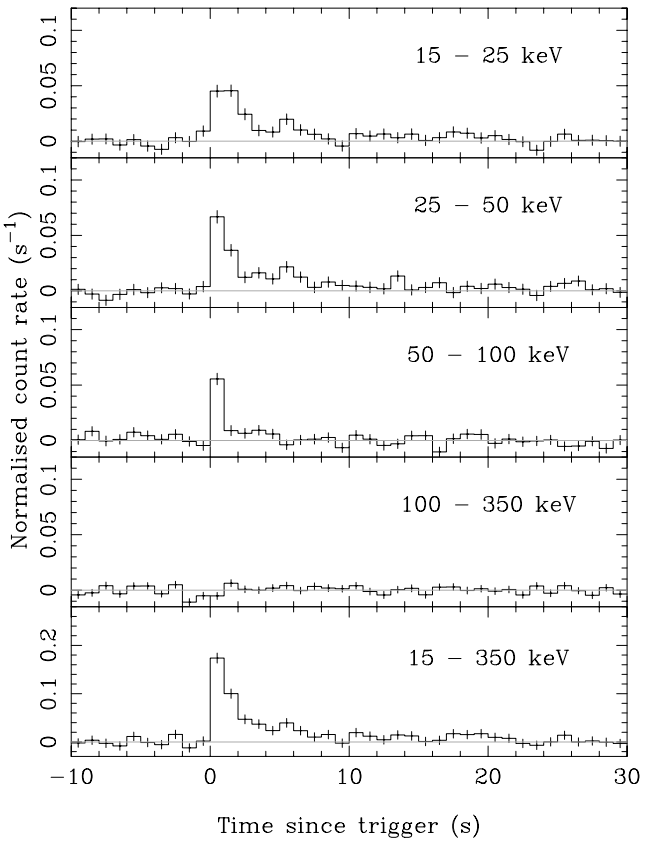

Figure 1. The GRB 050801 BAT light curve. From top to bottom: light curves in the 15–25, 25–50, 50–100, 100–350 and 15–350 keV energy bands. Units on the *Y*-axis are counts per second per detector.

we present the X-ray, optical and UV observations performed with *Swift* and we discuss the multiwavelength properties of the GRB 050801's afterglow.

3 *Swift* X-RAY AND OPTICAL OBSERVATIONS OF GRB 050801

Following the BAT trigger, GRB 050801 was observed by the XRT and UVOT instruments. A bright, unknown X-ray and optical source was found inside the BAT error circle, at coordinates RA = 13:36:35.4, Dec. = −21:55:42.3 (as measured with UVOT). This source subsequently faded, and it was therefore confirmed as the afterglow of this burst. Other prompt optical observations were successfully performed with ROTSE (Rykoff et al. 2006), and further observations were made by Fynbo et al. (2005a,b), 6 and 30 h after the burst onset, respectively. No radio afterglow was detected (Cameron et al. 2005).

The UVOT began observing the field of GRB 050801 52 s after the BAT trigger. The first ∼9.4-s exposure, taken while the spacecraft was settling on the target, was taken through the *V* filter in photon-counting ('event') mode. Once the pointing had stabilized, a 100-s *V*-band finding-chart exposure in combined image and event mode was taken. After this, the UVOT cycled through the colour filters, firstly with 10-s exposures, then 100 s and finally 900 s. The later exposures were taken in image mode (IM) only.

A series of images were created from the settling and finding chart event lists. A single image was produced from the settling exposure, and the 100-s finding-chart event list was used to produce 11 time-sliced images. The first two of these images have 5-s exposure times, and the next nine images are of 10-s duration. Counts were extracted from the images in all filters using a 4 arcsec radius aperture at the position of the afterglow. A 25 arcsec radius region, offset from the source, was used to determine the background count rates. The source count rates were aperture-corrected to a 6 arcsec radius to ensure compatibility with the photometry calibration (Poole 2005), and were corrected for detector dead-time and coincidence loss (i.e. lost counts due to multiple photons arriving in a single region of the detector within a single frame). The count rates were converted to magnitudes and fluxes using, respectively, the zero-points and counts-to-flux conversions available in the *Swift* CALDB. The complete log of UVOT observations is shown in Table 1.

Observations using the XRT began approximately 61 s after the burst trigger. The first exposure, taken in the IM, did not show any source. Subsequently, the XRT observed in windowed timing (WT) mode for approximately 20 s. This observational mode did not accumulate enough counts to produce any useful spectral information. The light curve was obtained from WT event data using XSELECT with 53 arcsec wide extraction slices for the source and background.

The rest of the XRT data were obtained in photon counting (PC) mode. The initial PC exposure lasted approximately 880 s and was found to be piled up. Comparison of the observed point spread function of the source to the model XRT point spread function indicated that significant pile up is restricted to the inner 7 arcsec radius region. Therefore source spectra and light curves were extracted from an annulus with an inner radius of 7 arcsec and an outer radius of 71 arcsec. Later data did not suffer from pile up and the extraction region was a circle of radius 70.7 arcsec. The background extraction region was taken as a circle of radius 189 arcsec for both the piled-up and the non-piled-up data. An additional fainter source was found within the extraction region and this was excluded for both the source and the piled-up extraction regions with a radius of 2.5 arcsec. For the PC mode data we included events of grade 0–12, in which the charge is spread over $\leqslant$4 pixels on the detector. The total exposure integration time in PC mode was 2.3×10^4 s. For the first day of observations a hot column in the XRT was close to the centre of the source, while at later times *Swift* was repointed to move the source away from this artefact. For spectral analysis we used the response matrix from the latest *Swift* calibration data base, CALDB 20051201, and the tasks xrtexpomap and xrtmkarf were used to produce effective area files, corrected for the hot column. The pileup correction factor was also taken from the arf files. This correction factor was dependant upon the distance of the burst centre to the hot pixel columns.

Fig. 2 shows the X-ray light curve of GRB 050801 in the 0.2–10 keV energy band. The optical/UV light curve is shown in Fig. 3; the optical emission of GRB 050801 does not decline in the first ∼200 s, after which it begins a systematic decay. This behaviour is very similar for the light curves in all filters, indicating no variation in the optical spectrum. We fitted the whole data set of optical/UV data points, which have been normalized to the *V* band (Fig. 3), with a broken power law. In the following we use the convention $F \propto t^{-\alpha}\nu^{-\beta}$, where F, t and ν are the flux, the time since the BAT trigger and the photon energy, respectively. The best-fitting values of the parameters are: an initial decay slope $\alpha_{\rm O,1} = 0.17 \pm 0.09$, a break time $t_{\rm O,b} = 230 \pm 15$ s and a late decay slope $\alpha_{\rm O,2} = 1.18 \pm 0.05$. The X-ray flux also lacks a strong decline ($\Delta \log F < 0.5$) in the first ∼200 s, but decays after this with a rate similar to that of the optical light curve. By fitting this light curve with a broken power law, we obtain an initial decay slope $\alpha_{\rm X,1} = -0.23 \pm 0.24$, a break time

Table 1. UV observations of GRB 050801 with UVOT in different time intervals after the BAT trigger. Errors are at 68 per cent C.L. For those observations where no source was found with at least 2σ significance, we list upper limits at 3σ.

Filter	$T_{\rm mid}$	$T_{\rm range}$	$T_{\rm exp}$	Magnitude
V	57	52–61	9.4	14.91 ± 0.07
V	67	64–69	5.0	14.5 ± 0.1
V	72	69–74	5.0	14.8 ± 0.1
V	79	74–84	10.0	15.13 ± 0.09
V	89	84–94	10.0	15.07 ± 0.08
V	99	94–104	10.0	15.08 ± 0.09
V	109	104–114	10.0	14.91 ± 0.08
V	119	114–124	10.0	15.05 ± 0.09
V	129	124–134	10.0	14.89 ± 0.08
V	139	134–144	10.0	15.19 ± 0.09
V	149	144–154	10.0	15.34 ± 0.09
V	159	154–164	9.8	14.92 ± 0.08
V	244	239–248	9.8	15.4 ± 0.1
V	328	323–333	9.8	15.25 ± 0.09
V	412	408–417	9.8	15.5 ± 0.1
V	497	492–502	9.8	16.1 ± 0.1
V	581	576–586	9.8	16.2 ± 0.1
V	666	661–671	9.8	16.8 ± 0.1
V	750	745–755	9.8	16.6 ± 0.1
V	835	830–840	9.8	16.7 ± 0.1
V	919	914–924	9.8	16.6 ± 0.1
V	5965	5515–6415	899.8	>19.3
V	35 314	17 583–53 044	2697.6	>20.6
V	149 467	108 434–190 500	4211.8	>20.0
B	215	210–220	9.8	15.32 ± 0.06
B	299	294–304	9.8	15.57 ± 0.06
B	383	379–388	9.8	16.13 ± 0.08
B	468	463–473	9.8	16.29 ± 0.08
B	553	548–557	9.8	16.37 ± 0.08
B	637	632–642	9.8	16.99 ± 0.09
B	721	717–726	9.7	16.60 ± 0.08
B	806	801–811	9.8	17.06 ± 0.09
B	890	885–895	9.8	17.19 ± 0.09
B	972	970–973	3.3	17.1 ± 0.2
B	33 617	15 767–51 466	3599.1	>21.1
U	201	196–205	9.8	14.35 ± 0.06
U	285	280–290	9.8	14.71 ± 0.07
U	369	365–374	9.7	15.04 ± 0.08
U	454	449–459	9.8	15.02 ± 0.08
U	538	533–543	9.8	15.5 ± 0.1
U	623	618–628	9.8	15.7 ± 0.1
U	707	702–712	9.8	15.9 ± 0.1
U	792	787–797	9.8	16.0 ± 0.1
U	876	871–881	9.8	15.6 ± 0.1
U	961	956–965	9.8	16.3 ± 0.1
U	12 159	11 773–12 545	771.3	19.30 ± 0.02
U	35 301	23 342–47 259	2114.0	20.99 ± 0.01
*UVW*1	187	182–192	9.8	14.7 ± 0.1
*UVW*1	271	267–276	9.8	15.0 ± 0.1
*UVW*1	356	351–361	9.8	15.4 ± 0.2
*UVW*1	440	435–445	9.8	15.4 ± 0.2
*UVW*1	525	520–530	9.8	15.8 ± 0.2
*UVW*1	609	604–614	9.8	16.0 ± 0.2
*UVW*1	694	689–698	9.8	16.6 ± 0.2
*UVW*1	778	773–783	9.8	15.8 ± 0.2
*UVW*1	862	858–867	9.8	16.9 ± 0.3
*UVW*1	947	942–952	9.8	16.14 ± 0.2
*UVW*1	11 316	10 866–11 766	899.8	19.18 ± 0.04
*UVW*1	34 511	22 435–46 587	2699.3	>20.6

Table 1 – *continued*

Filter	$T_{\rm mid}$	$T_{\rm range}$	$T_{\rm exp}$	Magnitude
*UVM*2	173	168–178	9.8	14.7 ± 0.2
*UVM*2	257	252–262	9.8	14.9 ± 0.2
*UVM*2	342	337–346	9.8	15.1 ± 0.2
*UVM*2	426	421–431	9.8	15.9 ± 0.3
*UVM*2	511	506–515	9.8	16.2 ± 0.3
*UVM*2	595	590–600	9.8	16.0 ± 0.3
*UVM*2	679	674–684	9.8	16.3 ± 0.3
*UVM*2	764	759–769	9.8	16.5 ± 0.4
*UVM*2	848	843–853	9.8	17.8 ± 0.5
*UVM*2	933	928–938	9.8	17.4 ± 0.5
*UVM*2	6590	6422–6759	337.1	18.7 ± 0.1
*UVM*2	10 415	9966–10 864	897.3	19.4 ± 0.07
*UVM*2	39 067	21 527–56 607	2910.5	>20.6
*UVW*2	230	225–235	9.8	16.1 ± 0.2
*UVW*2	314	309–319	9.8	16.6 ± 0.3
*UVW*2	399	394–404	9.8	16.5 ± 0.3
*UVW*2	483	478–488	9.8	17.1 ± 0.3
*UVW*2	568	563–573	9.8	18.2 ± 0.4
*UVW*2	652	647–657	9.8	18.3 ± 0.5
*UVW*2	737	732–741	9.8	>17.9
*UVW*2	821	816–826	9.8	17.4 ± 0.4
*UVW*2	906	901–910	9.8	17.6 ± 0.4
*UVW*2	4524	4188–4859	670.6	20.2 ± 0.05
*UVW*2	34 525	16 676–52 374	3599.1	>21.6

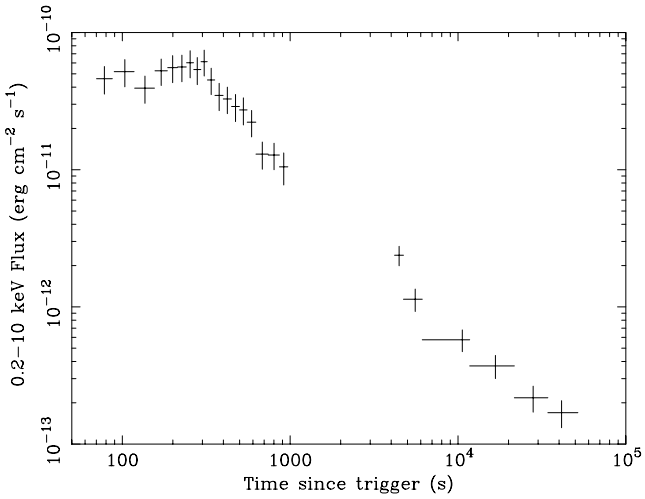

Figure 2. The GRB 050801 X-ray afterglow observed with *Swift* XRT in the 0.2–10 keV energy band.

$t_{\rm X,b} = 257^{+35}_{-24}$ s, and a late decay slope of $\alpha_{\rm X,2} = 1.22 \pm 0.04$: all these values are consistent with those obtained by fitting the optical light curve, within 2σ. In fact, we find that the optical-to-X-ray flux ratio remains remarkably constant throughout the whole observation (see Fig. 4). In order to formally assess that, we deconvolved the intrinsic distribution of our data from the distribution of measurement errors. We followed the maximum likelihood method of Maccacaro et al. (1988) to obtain the best estimate of the intrinsic s.d. $\sigma_{\rm M}$ of the optical-to-X ray flux ratio. We got $\sigma_{\rm OX,M} = 0.02^{+0.02}_{-0.01}$, which is consistent, within 1.5 s.d., with 0. The 3σ upper limit on intrinsic s.d. is 0.06.

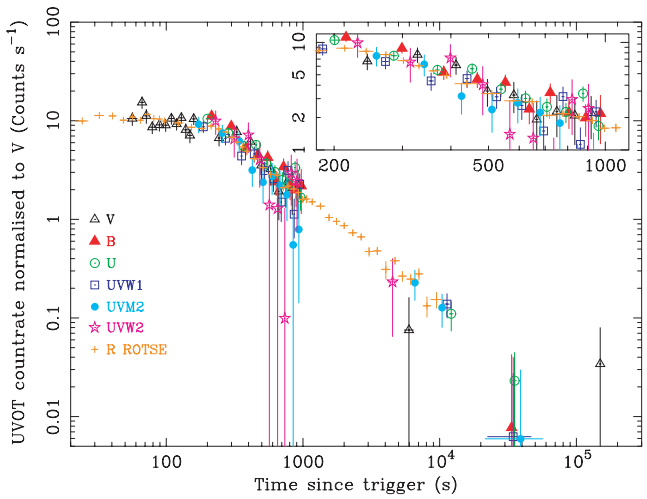

Figure 3. *Swift* UVOT count rate of GRB 050801 in all filters, renormalized to the *V* band. We also show the ROTSE *R*-band points, renormalized with the same criterion.

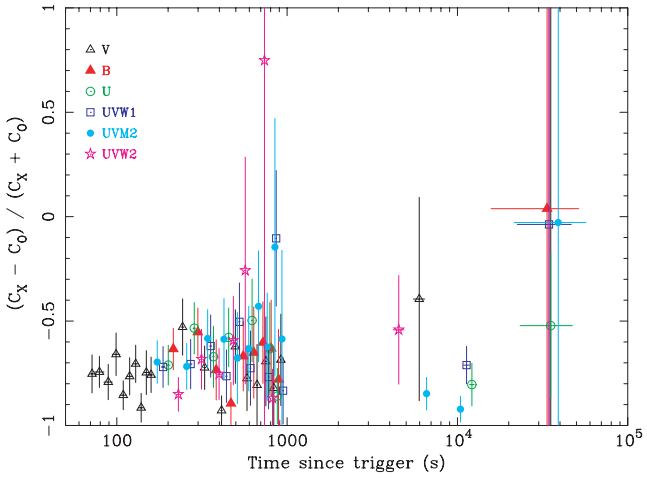

Figure 4. Ratio of the *Swift* XRT and UVOT count rate (renormalized). The ratio is defined as $(C_X - C_O)/(C_X + C_O)$, where C_X and C_O are the count rates in the XRT and a given UVOT filter, respectively.

We also note that the level of the optical flux found by ROTSE 22 s after the trigger (Rykoff et al. 2006) is consistent with the plateau we find 70–230 s after the trigger, indicating that the optical flux was roughly constant for ∼200 s after the end of the prompt emission.

The 0.2–10 keV spectrum obtained with XRT is well fitted with an absorbed power-law model; results are listed in Table 2 and Fig. 5. There is no evidence for spectral evolution during the whole of the follow-up observation. This is confirmed by the fact that there is no change in the softness ratio, as shown in Fig. 6. By means of the maximum likelihood method of Maccacaro, we found that the best estimate of the intrinsic dispersion of softness ratio is $\sigma_{S,M} = 0.075 \pm 0.062$, which is consistent with 0 at 1.1σ level.

The similar behaviour of the X-ray and optical light curves, as well as the absence of any change in the spectral properties, suggests that these two bands both lie in the same spectral segment. In order to test this hypothesis, and to understand the spectral properties of the burst in more detail, we reconstructed the spectral energy distribution (SED) between these bands, spanning ∼4 decades in frequency.

We performed a joint spectral fit of optical and X-ray data taken between 160 and 970 s after the burst (i.e. where both X-ray and optical flux were highest). We fitted the spectra with a power-law model, which is widely assumed to be the spectral shape of GRB emission, and we have included the effects of photoelectric absorption using the phabs and zphabs models in sc xspec. In our fit, phabs is fixed at the Galactic value $N_H = 7 \times 10^{20}$ cm^{-2} (Dickey & Lockman 1990), while zphabs is allowed to vary. The optical/UV data points were corrected for the Galactic dust extinction before reading into XSPEC, by using the Galactic extinction law reported in Seaton (1979). Such a multicomponent model gives a rough reproduction of the whole spectrum, with $\chi^2_{nu} = 38.4/27$ (see Fig. 7). The best-fitting value of the optical to X-ray spectral index is $\beta_{OX} = 0.85 \pm 0.02$, which is consistent with the spectral slope in the X-ray band, supporting a scenario in which the X-ray and optical data lie on the same spectral segment.

Joint analysis of the optical and X-ray data has also allowed us to derive a photometric redshift z for the burst; no spectroscopic redshift is available. Extragalactic hydrogen will cause a dropout in the emission blueward of $91.2(1 + z)$ nm, which can be detected by *Swift* UVOT if $z > 1$. In the case of GRB 050801, there is a dramatic difference in flux between the *UVM2* and *UVW2* filters, (see Fig. 7), and from the fit described above, we formally obtain $z = 1.56 \pm 0.06$. We should, however, note that the spectral model we used includes the sharp cut-off at the Ly-limit, $91.2(1 + z)$ nm, but does not include the Lyα forest, or Lyα absorption from the host galaxy of the GRB. Together, these two sources of Lyα absorption will erode the spectrum between 121.6 and $121.6(1 + z)$ nm, suggesting that the true redshift might be slightly below the value we determined and increasing the uncertainty on the redshift beyond the statistical errors on the model fit. At redshift ∼1.6, Lyα from intervening systems is expected to absorb less than 10 per cent of the broad-band flux (Madau 1995), and will only influence the photometry in the UV filters of the UVOT. As this attenuation is smaller than the

Table 2. Best-fitting parameters for the X-ray spectrum of GRB 050801 in different time intervals after the BAT trigger. WT data analysis results are not shown because of the low statistics. Errors in β are at 68 per cent C.L., while N_H upper limits are reported at 90 per cent C.L. and at $z = 0$. The values of N_H represent the excess absorption above the Galactic value of 7×10^{20} (Dickey & Lockman 1990).

Segment	Energy index β	N_H ($\times 10^{22}$ cm^{-2})	Time interval (s)
Plateau (piled-up data)	0.79 ± 0.23	–	90–300
Whole piled-up PC data	0.70 ± 0.12	<0.05	90–975
Non-piled-up PC data	0.87 ± 0.23	<0.06	4097–52 950

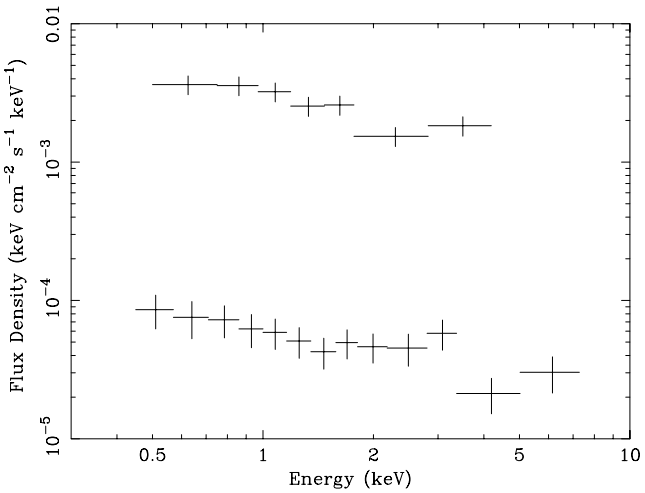

Figure 5. The GRB 050801 X-ray spectrum during the piled-up phase (time interval 90–975 s, top points) and the non-piled-up phase (since 975 s, bottom points).

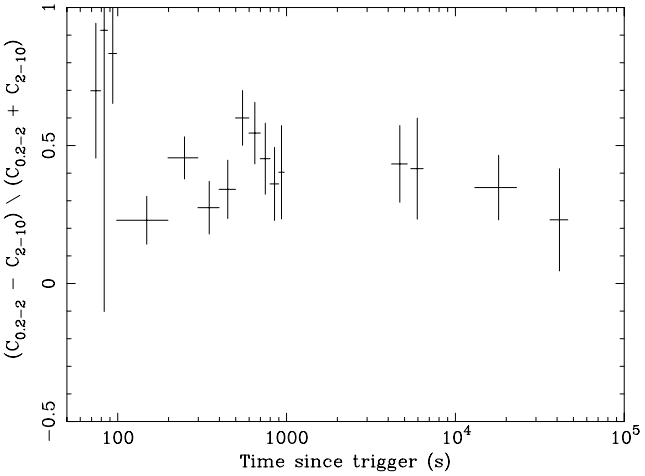

Figure 6. Softness ratio of X-ray data, defined as $(C_{0.2–2} - C_{2–10})/(C_{0.2–2} + C_{2–10})$, where $C_{0.2–2}$ and $C_{2–10}$ are the count rate in the 0.2–10 keV band and in the 2–10 keV band, respectively.

statistical uncertainty on the UV data points (15, 23 and 28 per cent for *UVW*1, *UVM*2 and *UVW*2, respectively), we consider a more realistic uncertainty for the redshift to be 0.10.

Despite these caveats, our photometric redshift should be close enough to the actual value to permit an adequate estimation of the energy emitted by GRB 050801 during its prompt emission phase. In calculating this energy we have taken the *K*-correction into account using the method of Bloom, Frail & Sari (2001), extrapolating the flux to energies below the BAT threshold. Assuming that the energy index does not change for $E < 15$ keV, we find the energy released over the 15–150 keV band (and in the GRB rest frame) to be 2.3×10^{51} erg. This value puts GRB 050801 in the low-energy tail of the GRB prompt energy distribution (Nousek et al. 2006; O'Brien et al. 2006). Assuming that the spectrum of the γ-ray emission does not change at higher energies, we calculate the total isotropic equivalent energy of this burst in the 1–10 000 keV band to be 9.16×10^{51} erg.

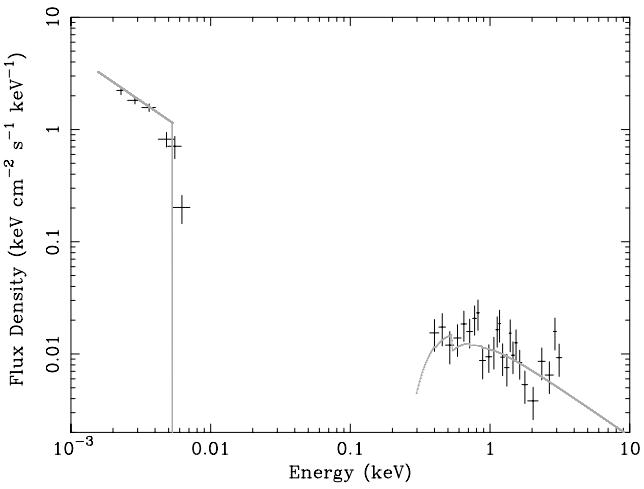

Figure 7. SED of GRB 050801, from*Swift* XRT and UVOT data. The best-fitting model is also plotted. In this figure, the model and XRT data points were obtained by unfolding the best-fitting model in XSPEC. The optical/UV flux densities were obtained by multiplying the UVOT count rates by the standard count rate-to-flux conversion factors (Poole 2005).

4 DISCUSSION

4.1 Onset of the afterglow

4.1.1 Constraints on the energy injection mechanism

The main peculiarity of the afterglow of GRB 050801 is the broad plateau observed at all wavelengths from optical to X-ray during the early phase. As we can see from Fig. 2, the X-ray emission is practically constant for ∼200 s, with a ratio between duration δt and time t which is nearly 1. There is no evidence for sharp decays or X-ray flares such as those observed in several *Swift* GRBs (Burrows et al. 2005; Nousek et al. 2006), which are usually associated with 'internal shocks' between the ultrarelativistic shells emitted by the central engine.

Among the various scenarios that can explain the observed plateau there are models in which the energy distribution over the fireball surface is non-uniform; these include the 'patchy jet' models (Kumar & Piran 2000) and the 'two component' jet models (Zhang, Woosley & Heger 2004). In the first case, the assumption is that the burst emission is released in a jet with large fluctuations in angular direction, that is, with a patchy distribution of Lorentz factor γ. Emission from different patches becomes observable at different times, according to their diverse values of γ^{-1}, and this can produce features which are observed in all bands almost simultaneously (as in GRB 050801). It should however be noted that the presence of large fluctuations of energy across the ejecta is still speculative, and that in order to give rise to early (<300-s) bumps, a distribution over a very narrow angular scale ($\theta \sim 0.^{\circ}1$) is required. Moreover, theoretical predictions show that in this scenario the 'bump' should follow a broad peak (see Zhang et al. 2006a). There is no indication of this in the available data.

The 'two component jet' model assumes the existence of two components in the ejecta: one ultrarelativistic component powering the GRB, and a second – moderately relativistic – cocoon component. The cocoon is decelerated later than the ultrarelativistic component because of its lower Lorentz factor (see Mészáros & Rees 2001; Ramirez-Ruiz et al. 2002; Zhang & Mészáros 2004). Its afterglow emission would therefore start later and may give rise to a

'bump' in the afterglow light curve. However, in accordance with the theoretical models mentioned above, such a feature should only be visible later than $\sim 10^4$ s (Zhang et al. 2006a).

The possibility we favour is that the plateau seen in both the X-ray and optical flux corresponds to the early afterglow, that is, to the phase that follows the creation of an 'external shock' after the fireball runs into the circumburst medium. The standard afterglow model predicts that, as a shell of ejecta interacts with the circumburst medium, it gives rise to a 'forward shock', which propagates outward. In its simplest formulation, the model predicts the production of a broad and achromatic flare, rather than a plateau, both in the optical and X-ray bands. The non-decay of the afterglow emission of GRB 050801 before 250 s after the trigger might then be explained by assuming that the central engine continues to inject radiative energy into the fireball for a few hundreds or even thousands of seconds after the initial explosion (late 'central engine' activity, Zhang & Mészáros 2002). As the emission from the central engine stops, the afterglow decay rate steepens up to more typical values. Assuming that the luminosity of the central engine scales as $L \propto t^{-q}$, the predicted relation between the decay and spectral slope is (Zhang & Mészáros 2002):

$$\alpha = \left(\frac{q}{2+1}\right)\beta + q - 1, \tag{1}$$

provided that the energy band we are dealing with is between the synchrotron peak frequency $\nu_{\rm m}$ and the cooling frequency ν_c.[1] As we will show later, this is indeed the case for both the optical and the X-ray observed frequencies. As for the decay index, we used the weighted average of $\alpha_{\rm X,1}$ and $\alpha_{\rm O,1}$, which is $\alpha_{\rm w} = 0.12 \pm 0.09$. For the spectral slope, we used $\beta_{\rm OX} = 0.85 \pm 0.02$. From this choice we obtained $q = 0.19 \pm 0.07$.

This value of q is consistent with 0 within 3σ, and interestingly such a flat luminosity distribution is expected in models in which the γ-ray burst leads to the birth of a millisecond pulsar with an ultrastrong magnetic field, that is, a so-called 'magnetar' (see e.g. Dai & Lu 1998; Zhang & Mészáros 2001). If this is the case, several parameters of the newly born compact object can be determined. We will discuss this intriguing scenario in more detail in Section 4.1.2.

An observationally indistinguishable possibility is that the central engine activity is as brief as the prompt emission itself but, at the end of the prompt phase, the ejecta are released with different Lorentz factors (see Rees & Mészáros 1998; Sari & Mészáros 2000; Panaitescu et al. 2005). The slowest shells would catch up with the fastest ones, once the latter have been decelerated by interaction with the circumburst medium. The additional energy produced when the shells shock with each other would make the afterglow decay shallower than usual. In this case, assuming that the mass M of the ejecta follows the law $M(>\gamma) \propto \gamma^s$, where γ is the shell's Lorentz factor, one can find an effective s value that mimics the effects of continuous energy injection with the luminosity law $L \sim t^{-q}$. Following Zhang et al. (2006a), this is,

$$s = -\frac{10 - 7q}{2 + q} \tag{2}$$

and therefore the value of q inferred above is equivalent to $s = -4.4 \pm 0.4$, that is, a very steep distribution. A steep distribution in the shells' Lorentz factors is required in order to have significant energy injection into the blast wave, with more energy carried by slow shells. Furthermore, the shell injection must occur over a suitably extended time interval in order to produce a flat plateau instead of a flare.

As mentioned previously, both these interpretations hold if the band where observations are taken is positioned between $\nu_{\rm m}$ and $\nu_{\rm C}$. This can be inferred by means of the 'closure relationships', which link the value of the spectral index in a given band with the decay index of the flux in the same band, according to the standard afterglow scenario (for a review, see Zhang & Mészáros 2004). These relationships are different depending upon the frequency range of the observed band, the density profile of the circumburst medium (constant as in the interstellar medium, or radially decreasing outwards from the centre of the explosion as expected in the case of a wind from a massive GRB progenitor), and on whether the ejecta expand spherically or in the form of a jet.

After the end of the plateau phase, in which (according to our interpretation) the behaviour of the afterglow is altered by late-time energy injection, one of these relationships should be satisfied if we assume that the afterglow behaves as theoretically predicted. In the case of the optical and X-ray afterglow of GRB 050801, we find that the only closure relationship which is satisfied is $\alpha = (3/2)\beta$ – which corresponds to the case of a spherical expansion of the ejecta into a constant density medium – and observing frequency ν satisfying $\nu_{\rm m} < \nu < \nu_c$. This also allows us to obtain a value for p, the power-law index of the energy distribution of the radiating electrons. On theoretical grounds, and for this spectral segment, it is $\alpha = (p-1)/2$ which gives $p = 2.70 \pm 0.05$.

4.1.2 Birth of a magnetar?

According to Zhang & Mészáros (2001), when the core of the stellar progenitor collapses into a pulsar, the luminosity emitted in the form of Poynting flux, L_0, is given by

$$L_0 = I\,\Omega_0^2\,2T_{\rm em} \sim 10^{49} B_{15}^2 P_{-3}^{-4} R_6^6 \ {\rm erg\,s^{-1}}, \tag{3}$$

where we use the convention $Q_x = Q/10^x$. In the above expression, I, Ω_0, P, R and B are, respectively, the neutron star's moment of inertia, initial angular velocity, initial period, radius and initial magnetic field. The quantity $T_{\rm em}$ represents the time-scale over which the emitted luminosity is roughly constant at the level L_0; following again the same authors, it is given by

$$T_{\rm em} = \frac{3c^2 I}{B^2 R^6 \Omega_0^2} = 2.05 \times 10^3 \left(I_{45} B_{15}^{-2} P_{-3}^2 R_6^{-6}\right) {\rm s}. \tag{4}$$

After the time $T_{\rm em}$, the model predicts a sharp cut-off of luminosity L, which decreases as $L \sim t^{-2}$, that is, $q = 2$. From Zhang & Mészáros (2001), the afterglow dynamics can be affected only if $q < 1$. Therefore, after the $T_{\rm em}$, we have no further modification of afterglow light curve due to energy injection.

By multiplying equation (3) with (4), we can estimate the amount of energy that is produced by the newly born neutron star and subsequently injected into the ejecta via dipolar spin-down. We get

$$L_0 T_{\rm em} = 2.05 \times 10^{52} P_{-3}^{-2} \ {\rm erg}. \tag{5}$$

Our data also allow us to estimate the change in kinetic energy, $E_{\rm K}$, during the 'plateau' phase. In the case where the observing frequency is between the peak frequency and the cooling frequency, the kinetic energy released as a function of the time is given by

[1] Note that the signs of the indices have been reversed with respect to the original paper by Zhang & Mészáros (2002), in order to make them consistent with our convention (here both α and β are positive).

(Zhang et al. 2006b)

$$E_{\rm K,52} = \left[\frac{\nu_{18} F(\nu = 10^{18}{\rm Hz})}{6.5 \times 10^{-31}}\right]^{4/(p+3)} D_{28}^{8/(p+3)} \times (1+z)^{-3(p-1)/(p+3)} t_{\rm d}^{3(p-1)/(p+3)} f_{\rm p}^{-4/(p+3)} \times \epsilon_{B,-2}^{(-p-1)/(p+3)} \epsilon_{E,-1}^{4(1+p)/(p+3)} n^{-2/(p+3)} \nu_{18}^{2(p-3)/(p+3)}, \quad (6)$$

where F($\nu = 10^{18}$ Hz) is the flux density at $\nu = 10^{18}$ Hz, D is the luminosity distance, $t_{\rm d}$ the time in the observer's frame, $f_{\rm p}$ is a function of the index p of the power-law energy distribution of radiating electrons, ϵ_B is the fraction of the energy that is contained in magnetic fields, $\epsilon_{\rm E}$ is the fraction of the energy associated with radiating electrons, n is the particle density in the surrounding medium and ν is the frequency at which we are observing. Again, subindices indicate normalized quantities ($Q_x = Q/10^x$), while $t_{\rm d}$ is in units of days.

For a GRB at $z = 1.56$, assuming the cosmological parameters $H_0 = 70, \Omega = 0.3$ and $\Lambda = 0.7$, we find $D = 4 \times 10^{28}$ cm. For the following parameters we take fiducial values of $\epsilon_{\rm E} = 0.3$ (Freedman & Waxmann 2001), $\epsilon_B = 0.03, n = 10$ (Berger, Kulkarni & Frail 2003), $\nu = 10^{18}$ Hz, $p = 2.7$ and $f_{\rm p} = 0.1$ (the function $f_{\rm p}$ is plotted in Zhang et al. 2006b). Inserting the time duration of the plateau [$\Delta t_{\rm d}$ = (250–70) s $\approx 2.1 \times 10^{-3}$ d] into equation (6), and using the 0.2–10 keV flux, $F \approx 4 \times 10^{-10}$ erg cm^{-2} s^{-1}, we can infer the increase in kinetic energy during this phase. This gives $\Delta E_{\rm K} \approx 1.4 \times 10^{53}$ erg. Finally, under the simple assumption that all the electromagnetic (EM) energy emitted by the pulsar has been completely converted into the kinetic energy of the ejecta (we discuss more realistic scenarios below), we have $\Delta E_{\rm K} = L_0 T_{\rm em}$ and equation (5) gives the neutron star period, $P_0 \approx 0.4 \times 10^{-3}$ s.

We can now use the value of the spin period to estimate the emitted luminosity and the pulsar's magnetic field strength. In the cosmological rest frame of the GRB, the plateau duration is (250–70) $\times (1+z)^{-1} \approx 70$ s, which gives a good approximation for the quantity $T_{\rm em}$. From equation (5) we therefore obtain a luminosity $L_0 \approx 2 \times 10^{51}$ erg s^{-1} and, from equation (3), a stellar magnetic field of $B \approx 1.4 \times 10^{15}$ G (using a neutron star radius of 10 km). This value is in the range expected for ultramagnetized neutron stars ('magnetars').

The existence of a plateau in the light curve also requires the pulsar to have a significant effect on the energetics of the afterglow. This means that the energy injected by the pulsar before the beginning of the afterglow, which we set at a certain time T_0, must be a sizeable fraction of the total kinetic energy that is left for the ejecta after the prompt emission phase, $E'_{\rm K}$:

$$L_0 T_0 \gtrsim E'_{\rm K}. \quad (7)$$

To test whether this condition is met, let us consider the energy E_γ radiated in γ-rays during the prompt emission. The radiative efficiency of a GRB, defined by the relation $\eta_\gamma = E_\gamma/(E_\gamma + E'_{\rm K})$, gives a measure of how efficiently the GRB dissipates the total energy into radiation during the γ-ray emission phase. On theoretical grounds (Guetta, Spada & Waxman 2001) this efficiency is not expected to be very high, with typical values of $\eta_\gamma \sim 0.2$ which are in agreement with pre-*Swift* results (De Pasquale et al. 2006). More recent analysis indicates much higher efficiencies, up to 0.7–0.8, although these values are hard to accommodate within the standard 'internal shock' emission mechanism of GRB prompt emission. Assuming a conservative value of $\eta_\gamma = 0.2$, and taking $E_\gamma = 9.16 \times 10^{51}$ erg for GRB 050801 (see Section 3), we obtain $E'_{\rm K} = 3.6 \times 10^{52}$ erg. This means that the condition $L_0 T_0 \gtrsim E'_{\rm K}$ is met for $T_0 \gtrsim 20$ s.

Unfortunately, a precise estimate of T_0, the time of the beginning of the afterglow, is not possible. Based on our data, we can only state that T_0 must be less than $\sim$70 s, when *Swift* began its follow-up observations. Comparing with the BAT light curve, we suggest that the afterglow beginning might be identified as the time of the second peak in the prompt emission, which is $\sim$5 s after the first peak. As mentioned above, this peak is broad and clearly softer than the first peak, which is to be expected if the first peak were due to internal shocks and the second to afterglow emission. Such behaviour has already been observed in the prompt emission of several GRBs, such as GRB 970228 (for a review see Frontera et al. 2000). It is worth noting that, if the afterglow begins about $\sim$5 s after the trigger, the optical emission detected by ROTSE can be associated with the afterglow and connected with the flat optical light curve recorded by UVOT later on (as observed). This comes with the caveat, though, that since we do not know the behaviour of the GRB in X-rays in the interval 20–70 s after the trigger, we cannot be sure that the emission in this period is actually due to the forward shock.

We can, however, discuss the possibility that the energy injection, which shapes the early afterglow curve, begins at the time of first ROTSE observation, that is, 20 s after the trigger. In such a case, we obtain, from equation (5), that the energy injected is 1.26 higher than previously calculated. This in turn decreases the required initial period P by a factor of 1.12, that is, we obtain $P = 0.36$ ms. From equation (3), we can infer that the magnetic field would lower by a factor of 1.26, so we have $B \approx 10^{15}$ G. As we can see, there is not a big change in the values of the parameters derived.

Finally, we shall briefly discuss the consequences of a slightly incorrect estimate of the redshift, as previously presented. If the true redshift is slightly above the value we used, the value of L_0 and $T_{\rm em}$ estimated previously should be increased and diminished, respectively. For small corrections of z, the product of these two parameters (see equation 5) does not vary largely. In addition, P has a weak dependence on this product. Therefore, we do not expect a large variation of P. For example, if the true redshift were 10 per cent lower than the value we reported, the value of P should increase only by 3 per cent. Conversely, if the true redshift were 10 per cent higher than that we found, P should be 3 per cent lower. Similarly, we do not predict a noticeable variation of the magnetic field. From equation (3), we can infer that the value of B_{15} would change by $\sim$1 per cent for a 10 per cent variation of the redshift. In the same way, the condition expressed by equation (7) is still satisfied in our model, for small changes in z without any considerable change of T_0.

4.1.3 Critical issues

The discussion presented in Section 4.1.2 is based on a number of assumptions regarding the parameters which describe the physical properties of the GRB. We note, however, that the dependence of the kinetic energy of the ejecta on $\epsilon_{\rm E}, \epsilon_B$ and n is not very strong, and so different values are not expected to significantly affect our conclusions. On the other hand, the assumption that all of the EM energy radiated by the pulsar is converted into the kinetic energy of the ejecta is more questionable. In a more realistic scenario, we would expect that only a fraction of this EM energy is converted in this way; in order for our scenario to be consistent, the efficiency cannot be lower than $\sim$30 per cent. We certainly do not expect the conversion efficiency to be too low, however, since the relatively low-energy emission from the magnetar is unable to penetrate the

shockwave. The Poynting flux energy of the pulsar can therefore only propagate outwards by conversion into the kinetic energy of the ejecta. The constraints regarding the conversion of the EM energy may be somewhat further eased if we assume that the ejecta outflow is moderately beamed. While such a condition would not be in contradiction with the observations or theory, it would further reduce the energy contribution required from the pulsar.

Other uncertainties relate to the way in which the pulsar energy injection is estimated. We assume that the magnetic field is constant during the phase in which energy injection is associated with the rapid pulsar spin-down, while in a more realistic scenario the coupling between rotational and magnetic evolution should be accounted for. Moreover, the emitted EM energy is calculated under the simple assumption of dipolar emission in vacuum, which is obviously a crude approximation during the first phases of neutron star formation and evolution. Dynamo effects, the presence of magnetospheric currents or multipolar components of the magnetic field may complicate this simple picture.

Our overall conclusion is that, to a first-order approximation, EM energy injection from a rapidly spinning magnetar (a neutron star rotating with a period of a few tenths of a millisecond and possessing an ultrastrong magnetic field of order $\sim 10^{15}$ G) can plausibly explain the observed plateau in the X-ray and optical light curves of GRB 050801. Although we have not directly derived estimates of the burst's physical parameters ($\epsilon_{\rm E}, \epsilon_B$, density of surrounding medium), the assumption of canonical values for these quantities is an adequate approximation for the purposes of our calculations.

It is instructive to compare GRB 050801 with the short GRB 051221 Fan & Xu (2006). In this latter event, a flattening occurred in the X-ray light curve between 3×10^3 and 2×10^4 s after the trigger. Optical data on this burst are rather sparse, and so cannot help constrain the afterglow physics. In the context of short GRBs, which are thought to arise from the coalescence of a binary system composed of two compact objects (such as two neutron stars or a neutron star and a black hole), it is difficult to imagine that the fall-back accretion of part of the material on to the central compact remnant can, hours after the coalescence, pump the emitted energy up to 10^{51}–10^{52} erg. Another scenario was therefore put forward in which two neutron stars coalesce and form a magnetar. In this hypothesis, the flattening of the light curve was interpreted as the signature of the underlying magnetar, whose energy injection can only significantly influence the afterglow light curve after several kiloseconds post-trigger. According to these authors, a magnetar with an initial period of 10^{-3} s and magnetic field of 10^{14} G can explain the observed behaviour. In the case of GRB 050801, we infer values for the period and magnetic field which are, respectively, shorter and higher. This is because, for this burst, the magnetar energy injection must occur over a shorter time interval, whilst the luminosity must be higher. It should be noted, nevertheless, that the differences in these parameters between the two GRBs are within $\sim$1 order of magnitude.

4.2 Absence of a reverse shock?

In the standard afterglow model, it is expected that the formation of a forward shock is accompanied by that of a less energetic 'reverse shock', which moves inward through the ejecta (Mészáros & Rees 1997). While the emission of the forward wave is predicted to peak in the X-ray band (at least at the early stages of the afterglow that we are considering here), the emission of the reverse shock should peak in the infrared–optical because of the higher density of the ejecta that it crosses.

In the case of GRB 050801, we do not observe any optical flares, and the optical emission always follows the X-ray emission, with the ratio of optical to X-ray flux remarkably constant (see Fig. 3). This suggests that the reverse shock emission is suppressed. A possible reason may be a very high magnetic field in the ejecta, in which case most of the energy is carried by the field itself and it is not converted into radiation in the shells. According to Zhang & Kobayashi (2005), for bursts with short duration (i.e. $t_{90} \lesssim 20$ s), suppression of the reverse shock takes place if the parameter σ, defined as

$$\sigma = \frac{B^{\rm e,2}}{4\pi n m_{\rm p} c^2}, \tag{8}$$

where $B^{\rm e}$ and n are the magnetic field and the density of the ejecta, respectively, and $m_{\rm p}$ is the proton mass, is larger than 100. The σ parameter can be interpreted as the ratio between the energy contained in the magnetic field and that in the baryonic outflow. Since the value of $B^{\rm e}$ is strongly dependent on the assumptions made about the position of the shock radius and the local particle density, it cannot be robustly determined. If internal shocks occur at small radii, even a relatively low magnetic field may prevent the reverse shock from forming. We can, however, give an order-of-magnitude estimate of $B^{\rm e}$ assuming an ejecta mass of 10^{-4} to $10^{-5}\,{\rm M}_\odot$, a shock radius at the onset of the afterglow of $r_{\rm sh} \sim 10^{13}$ cm and a spherical shell of depth $c\delta t$ with $\delta t \sim t_{90} \sim 20$ s. This gives a particle density of $n \sim 10^8$ cm^{-3} in the shell, which in turn implies a magnetic field of $B^{\rm e} \sim 10^4$ G. Another observational consequence of a strongly magnetized reverse shock is the broadening of its emission profile (Zhang & Kobayashi 2005). This phenomenon, together with the suppression of the peak emission, would make the reverse shock emission even less evident. It should be noted that the hypothesis of a high magnetic field in the ejecta may be consistent with the powering of the wind by a magnetar. Thus, the non-detection of a reverse shock component in the emission of this burst may be in agreement with the identification of the central engine of GRB 050801 as a magnetar.

Other scenarios are, however, also plausible. For example, we cannot exclude the possibility that, for unusually high density ejecta, the reverse shock emission would have peaked in the far-infrared rather than in the infrared or optical. In such a case, it would have made a negligible contribution to the emission detected by UVOT, which is consistent with our observations.

5 CONCLUSIONS

Swift GRB 050801 shows remarkable spectral and temporal features, in both the X-ray and optical/UV bands. Instead of rapidly decaying flux within 100–200 s after the trigger, as seen in the majority of bursts, the GRB 050801 emission in the X-ray and in the optical has a plateau from $\sim$70 s up to $\sim$250 s after the BAT trigger, followed by a more normal decay slope. It is possible that the plateau actually extends back to $\sim$20 s after the trigger, which could explain why the first prompt optical measurement, performed by ROTSE-III at this epoch, is consistent with the UVOT data.

We find that the relatively flat X-ray light curve might be caused by a late energy injection by the 'central engine' to the expanding shell, in the form of either Poynting flux or the shock dissipation that occurs when late shells catch up with earlier ones. In the case of energy injection due to Poynting flux, we have shown that dipolar spinning down emission from a newly born magnetar of initial period $P_0 \simeq 0.4$ s and magnetic field $B \simeq 1.4 \times 10^{15}$ G can account for the X-ray flux observed during the plateau phase and for its duration. Other models, which involve uneven energy distribution in

the ejecta or internal shock emission are likely to be ruled out by the fact that the plateau appears at early time and its emission is remarkably smooth.

The energy injection model requires that the afterglow has already started by the time of the *Swift* measurements. This hypothesis is supported by the fact that the optical-to-X-ray flux ratio during the plateau is consistent with that observed at late times, when the afterglow has certainly begun. We suggest that the afterglow onset might actually be associated with the second peak detected by BAT. This peak is very soft, as expected if it is connected with the afterglow emission, and it occurred only $\sim$5 s after the trigger.

Theory predicts that the forward shock in the circumburst medium, responsible for the afterglow emission, should be accompanied by a reverse shock that moves inwards through the ejecta. The reverse shock emission should be brief and peaked in the optical. On the other hand, the constancy of the optical to X-ray flux ratio observed during this event suggests that no reverse shock emission has taken place, at least during the *Swift* observations. The suppression of the reverse shock emission might suggest the presence of highly magnetized ejecta, in which most of the energy is carried by the magnetic field rather than the shock.

Finally, a joint fit of the X-ray and optical data has allowed us to confirm that data in both bands lay on the same spectral segment, between the synchrotron peak and the cooling frequency, and to determine the spectral index with high precision. Analysis of the late-time ($>$300 s) afterglow emission, based on the application of closure relations, suggests that the GRB fireball had a spherical expansion in a constant density environment. More importantly, we have been able to determine the redshift of the burst as $z = 1.56$.

ACKNOWLEDGMENTS

The authors wish to thank J. Osborne, P. Boyd, P. Schady and S. Kobayashi for the valuable comments that helped to improve the manuscript. SZ thanks PPARC for its support through a PPARC Advanced Fellowship.

REFERENCES

Barthelmy S. D. et al., 2005, Space Sci. Rev., 120, 143
Berger E., Kulkarni S. R., Frail D. A., 2003, ApJ, 590, 379
Bloom J. S., Frail D. A., Sari R., 2001, AJ, 121, 2879
Burrows D. N. et al., 2005, Space Sci. Rev., 120, 165
Cameron P. B. et al., 2005, GCN 3762 (online only reference: http://gcn.gsfc.nasa.gov/gcn3/3762.gcn3)
Dai Z. G., Lu T., A&A, 1998, 333, L87
De Pasquale M., Piro L., Gendre B. et al., 2006, A&A, 455, 813
Dickey J. M., Lockman F. J., 1990, ARA&A, 28, 215D
Fan Y., Xu D. 2006, MNRAS, 372, 19
Frail D. A., Kulkarni S. R., Sari R. et al., 2001, ApJ, 562, L55
Freedman D., Waxman E., 2001, ApJ, 547, 922
Frontera F., Amati L., Costa E. et al., 2000, ApJS, 127, 59
Fynbo J. et al., 2005a, GCN 3736 (online-only reference: http://gcn.gsfc.nasa.gov/gcn3/3736.gcn3)
Fynbo J. et al., 2005b, GCN 3743 (online-only reference: http://gcn.gsfc.nasa.gov/gcn3/3743.gcn3)
Guetta D., Spada M., Waxman E., 2001, ApJ, 557, 399
Jakobsson P. et al., 2006, A&A, 447, 897
Kumar P., Piran A., 2000, ApJ, 532, 286
Maccacaro T., Gioia I. M., Wolter A., Zamorani G., Stocke J. T., 1988, ApJ, 326, 680
Madau P., 1995, ApJ, 441, 18
Mészáros P., Rees M. J., 1997, ApJ, 476, 232
Mészáros P., Rees M. J., 2001, ApJ, 556, L37
Nousek J. et al., 2006, ApJ, 642, 389
O'Brien P. et al. 2006, ApJ, 647, 1213
Panaitescu A. et al., 2006, MNRAS, 366, 1357
Poole T. S., 2005, *Swift* CALDB release note. Online-only reference: http://swift.gsfc.nasa.gov/docs/heasarc/caldb/swift/docs/uvot/uvot_calb_counttofluxratio_01a.pdf
Ramirez-Ruiz E., Celotti A., Rees M. J., 2002, MNRAS, 337, 1349
Rees M., Mészáros P., 1998, ApJ, 496, L1
Roming P. et al., 2005, Space Sci. Rev., 120, 95
Rykoff E. S. et al., 2006, ApJ, 638, L5
Sari R., Mészáros P., 2000, ApJ, 535, L33
Seaton M. J., 1979, MNRAS, 187, 73
Zhang B., Meszaros P., 2001, ApJ, 552, L35
Zhang B., Meszaros P., 2002, ApJ, 566, 712
Zhang B., Meszaros P., 2004, Internat. J. Mod. Phys. A, 19, 2385
Zhang B., Kobayashi S., 2005, ApJ, 628, 315
Zhang B., Fan Y. Z., Dyks J., Kobayashi S., Mészáros P., Burrows D. N., Nousek J. A., Gehrels N., 2006, ApJ, 642, 354
Zhang B. et al., 2007, ApJ, 655, 989
Zhang W., Woosley S. E., Heger A., 2004, ApJ, 608, 365

This paper has been typeset from a TEX/LATEX file prepared by the author.